Nomenclature На Hartmann number (–) L_1,L_2 Dimensionless heat source length PrPrandtl number (–) B_0 Magnetic field (–) Greek symbols Specific heat (J kg⁻¹ K⁻¹) cConstant moving parameter λ. TTemperature (K) Thermal expansion coefficient (K^{-1}) β $Nu_{s.}$ Local Nusselt number (-) Density (kg m⁻³) ρ $Nu_{m.}$ Average Nusselt number (–) dynamic viscosity μ Thermal conductivity (W m^{-1} K $^{-1}$) k Kinematic viscosity (m²/s) Velocity components in x and ydirections, respecu, v Heat capacity ratio σ tively (m s⁻¹) solid volume fraction Reynold number (-) ReDimensionless temperature LAspect ratio (-) Pressure term (Pa) Subscripts Φ Magnetic angle f Base fluid GrGrashof number Nanofluid nf Height of cavity HSolid nanoparticles \boldsymbol{S} S Local entropy Top t Thermal performance factor eRight l_1, l_2 Heat source length

applications are energy storage systems [4–6], Heat exchangers [7–10], porous media [11,12], and solar collectors [13–14]. The very first idea for heat transfer was utilizing conventional fluids like water, oil, and ethyline glycol. These fluids had low thermal performance. Choi and Eastman [15] were the first ones to introduce adding nanoparticles to the base fluid (water). Their ultimate goal was to enhance thermal conductivity of water by adding metalic nanoparticles with higher amount of thermal conductivity.

There are three categories of convection heat transfer in nanofluids; natural convection, mixed convection and forced convection. During recent years, mixed convection is under consideration for various applications such as HVAC, bio convection and renewable energy. During recent years, scientists are becoming interested in analyzing the mixed convection in enclosures. Tiwari and Das [16] were the first to study mixed convection for nanofluids in enclosure. Mehmood et al. [17] utilized KKL model for the mixed convection of Al-H₂O nanofluid in a square porous cavity. They studied the impacts of non-linear mode of radiation and also the magnetic field effect. They demonstrated that the stream function increases when the porosity is increased. Other parameters such as the effects of wall physical properties on heat transfer are also studied in literature. Selimefendigil et al. [18] considered entropy generation in their study about the mixed convection of the nanofluid in a triangular shape enclosure with the rotational cylinder put inside the enclosure area. They studied the effects of Rayleigh number, cylinder rotational speed, nanofluid volume fraction parameter, and elastic modulus of the sidewall on average heat transfer. Different shapes of enclosures and the effect of magnetic field are another topics done be researchers. The study was done by Chamkha and Ismael [19] on mixed convection in trapezoidal enclosure. They remarked the concept of magnetic field for the mixture of water and Copper. The boundary conditions were; fixed left sidewall with the isothermal cold temperature, insulated bottom and top walls, and horizontally magnetic field. They

extracted the governing equations by method of finite element and stream function vorticity procedure. The grid sizes were (226*101, 230*71, and 285*51) and the inclination angles of the sidewall were (66, and 801). The other input parameters were Ricahrdson number (0.01–10), volume fraction (0–0.05), and Hartmann number (0–100). The results disclosed that if the sidewall's inclination angle increases, there will be higher average Nusselt number and the enhancement of the averaged Nusselt number is higher for the opposing lid-driven case.

Recently, a new method of heat transfer within nanofluids is introduced. The method is about the combination of two various nanoparticles or more in the primary fluid. These nanofluids are known as Hybrid nanofluid and have a superior heat transfer efficiency regarding their superior thermo-physical properties [20]. Asadi et al. [21] studied Al₂O₃-MWCNT/ oil hybrid nanofluid efficiency in the range of various temperatures (25–50 °C) and volume fractions (0.125%-1.5%). They utilized analysis of Zeta potential to investigate the consistency of the nanofluid. Thermo-physical parameters like dynamic vicosity, thermal conductivity, pumping power, convective heat transfer and the heat transfer's efficiency within the nanofluid were enhanced via increasing the the hybrid nanoparticles volume fraction for both the turbulent and laminar regimes. They also introduced correlations to assume the thermal conductivity and dynamics viscosity regarding their experimental data. Hybrid nanofluids are also used in open cavities. Entropy generation breakup is studied via Hussain et al. [22] about the MHD mixed convection action of Al₂O₃-Cu-Water Hybrid nanofluid in a cavity with open area. They tested three different locations of the adiabatic abstacle in the channel to see the heat transfer changes of the hybrid nanofluid. Other input parameters were Ricahrdson number $(0.01 \le Ri \le 20)$, Reynolds number, volume fraction of nanoparticle (0.0 $\leq \phi \leq$ 0.04), and Hartmann number $(1 \le Re \le 200)$, $(1 \le Ha \le 100)$. They deduced that the increase in Hartmann number, decrements the Average Nusselt number and entropy generation. They also showed that if the Richardson number goes up, the mixed convection, the rate of heat transfer and also the entropy generation increment. Porous media is used in different applications such as thermal insulation, and desalination systems. Gorla et al. [23] studied the Magnetohydrodynamic mode of natural convection for C-Al₂O₃/water hybrid nanofluid in porous square cavity considering the impacts of heat source/sink. They benefited Finite difference method to discrete the governing equations and also the upwind scheme to obtain solutions. Decrease in average Nusselt number by changing the place of heat source, decrease in velocity by incrementing the Hartmann number, and increase in local Nusselt number by increasing hybrid volume fraction were some of their results.

There are different base fluids which are used for hybrid nanofluids. Han et al. [24] and Botha et al. [25] benefited the oil to be the primary fluid for studying synthesizing hybrid nanofluids. The water based nanofluids were also studied by some researchers [26–31]. Nine et al. [32] utilized wet ball milling for Cu/Cu_2O -water hybrid nanofluid. The other mostly used base fluid is ehtylene glycol. Paul et al. [33] investigated the mixture of Zn and Al which were blended (Zink (5%) and aluminum (95%)). They used the two-step process and considered steady state nanofluid. Baby and Ramaprabhu [34–36] and Sunder et al. [37] also considered the Ethylene Glycol to be the base fluid in their studies.

Heat transfer characteristics and thermophysical properties of hybrid nanofluids are also investigated by some reaserchers. Jana et al. [26] studied two different water based hybrid nanofluids (CNT-AuNP and CNT-CuNP). They observed that by adding CNT to both CuNP and AuNP, the thermal con-

Table 1 Thermo-physical properties of copper, water, and Alumina [48]:

Property	Water	Copper (Cu)	Alumina (Al ₂ O ₃)
$\overline{\rho}$	997.1	8933	3970
C_p k	4179	385	765
k	0.613	401	40
	21×10^{-5}	1.67×10^{-5}	0.85×10^{-5}
	0.05	5.96×10^7	1x10 ⁻¹⁰

ductivity does not increase. Ho et al. [27] did the experimental study by measuring Al_2O_3/PCM -water hybrid nanofluid density from their theoretical mixture formula. Experimental analysis is also done on hybrid nanofluids by some researchers. Suresh et al. [38] provided the set up constructed from calming section, test section, cooling unit, reservoir, and pump to study heat transfer and also Al_2O_3 -Cu/water hybrid nanofluid pressure drop. They considered the flow in the tube as a fully developed, laminar and uniformly heated. Their results demonstrated 13.56% growth in Nusselt number compared to based water.

There are few works done about entropy generation regarding heat transfer within cavity. entropy generation is a criteria to evaluate the systems's performance especifically in heat transfer field of study. More entropy generation means more destruction of the available work and is a criterion for measur-

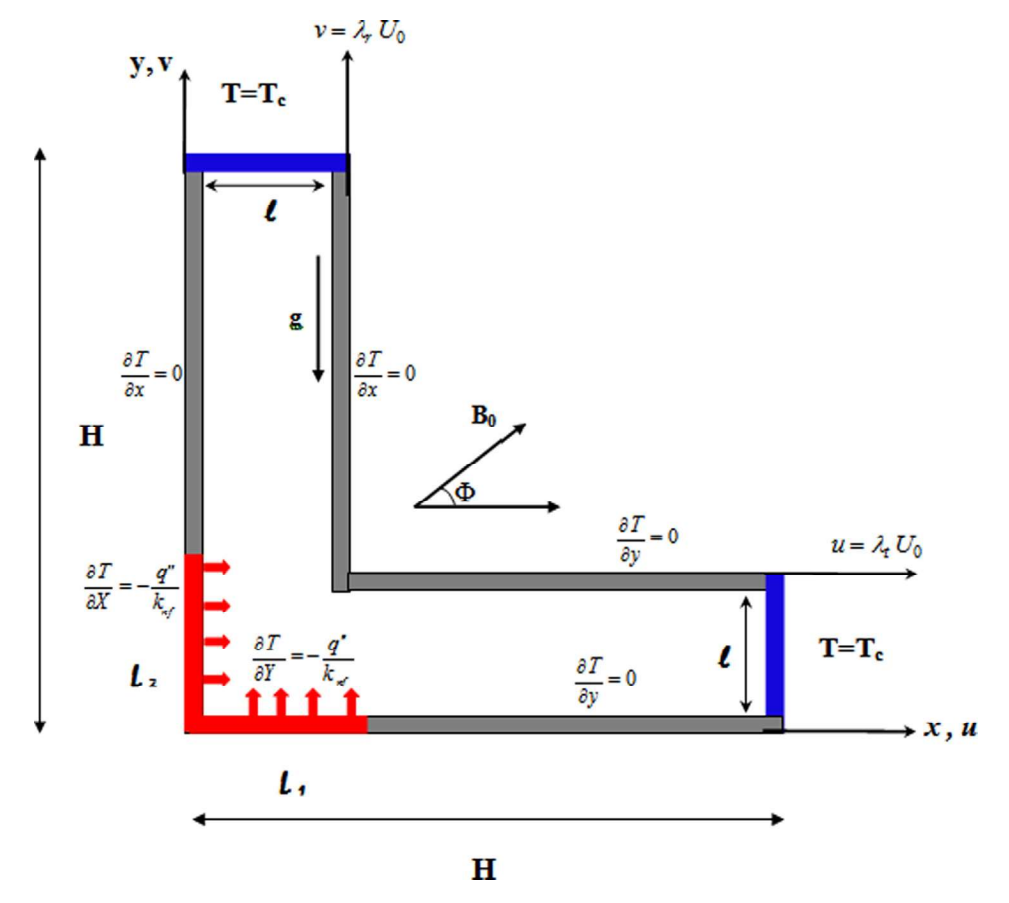


Fig. 1 Geometry of the problem.

ing the irreversibility. Rashad et al. [39] considered entropy generation of Cu-water in a porous enclosure. They studied entropy generation for various locations and sizes of source/sink and volume fractions of Cu nanoparticle. Their results approved that if the volume fraction increments, the entropy generation decrements which means the irreversibility of heat transfer reduces. Rashidi et al. [40] considered the impact of rotating disk, and the magnetic field on entropy generation. Armaghani et al. [41] did the noval study through the porous media in a cavity which was in different layers. For the two layers studied, they concluded that for high Rayleigh numbers, the only governing factor of entropy generation is the nanofluid layer.

Investigation of Magneto-hydrodynamic effect (MHD) on heat transfer is another interesting issue among researchers. Wagas et al. [42] searched the MHD and mixed convection in a liquid with nonlinear stretching surface. They used the nonlinear magnetic field. They demonstrated that the Lorentz force within magnetic parameter is stronger if the Hartmann number increases. Su et al. [43] studied the MHD and mixed convection on stretching wedge considering thermal radiation. They studied the impact of magnetic field for different numbers of velocity ratio parameter. The more the magnetic parameter, the more the absolute skin friction coefficient and the less the momentum boundary layer thickness. Mondal et al. [44] studied the effect of MHD mixed convection in a wall moving cavity (the upper cold wall moving) with porous media. They used Brinkman-Forchheimer-Darcy model to investigate streamlines, isotherms, and Nusselt number. They concluded that high values of Grashof number causes circulation of flow and increase in heat transfer. Moreover, they demonstrated that partial motion of wall has a direct effect on heat transfer rate. Biswas et al [45] studied the effect of free aspiration on magneto-thermal convection for three different

scenarios in a square cavity; Differentially heated cavity (DHCA), split-heated cavity (SHCA), and corner-heated cavity (CHCA). In order to model magnetic field, they used Maxwell model, and for porous media, they utilized Brinkman-Forcheimer-Darcy model. Their resuts demonstrated that the aspiration of flow stream hs the main role to remove heat from the heater in cavity for all of three scenarios. Some of the work done in literature have considered nonuniform heating for magneto-hydrodynamic thermal convection. Biswas et al. [46] studied the effects of half-sinusoidal and nonuniform heating of the bottom wall on natural convection heat transfer in an square enclosure. They used finite volume method to model and analyze the amplitude and spatial frequency of the half-sinusoidal heating on hybrid nanofluid heat transfer performance. Their results revealed that the amplitude has a direct relation with average Nusselt number, but the increaes in frequency of heating caused periodic oscillations in temperature which reduces local and average Nusselt number. The Marangoni convection is another form of heat transfer which is studied in literature for MHD flow. Biswas et al. [47] studied transient and steady state analysis of free, forced, and Marangoni convection for a square enclosure and with uniform magnetic field. The Marangoni convection happens when there is a thermal interaction at the open surface of the cavity. Some of their findings were; decreasing in size of marangoni circulations with the increase in Biot and Reynolds numbers, increase in magnetic filed force by increasing the Hartmann number, and high order of magnetic field influence on thermal mixing.

Considering the literature review presented in this paper, one can conclude that magnetohydrodynamic mixed convection is of interest for many researchers and is applicable in various fields of fluid mechanics. Although researchers studied many experimental and computational modes of mixed con-

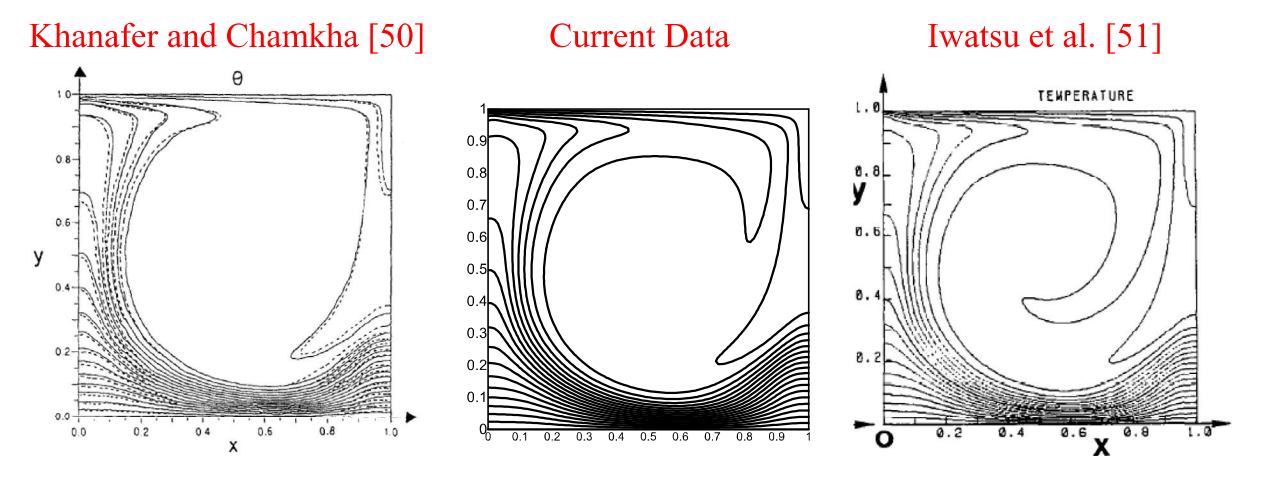


Fig. 2 Comparison plot with Khanafer and Chamkha [50] and Iwatsu et al. [51].

Table 2 Grid-independency study for hybrid nanofluid.							
Grid-size	41×41	61 × 61	81 × 81	91 × 91	101 × 101	121 × 121	
Nu_m	9.37966	9.57996	9.729889	9.9504381	9.990265	9.9906677	

Table 3 Comparisons of the average Nusselt number for several values of Re at. Pr = 0.71, $Gr = 10^2$.

Re	Khanafer and Chamkha [50]	Iwatsu et al. [51]	Current outcomes
100	2.01	1.94	1.93
400	3.91	3.84	3.91
1000	6.33	6.33	6.31

vection in cavities, there is a need to conduct more analysis in this field of study. Apart from that, there is a limited literature about hybrid nanofluids since they are new and unkown to many reaserchers. Though, different shapes of cavities are studied in literature, the L-shape cavity is investigated rarely by researchers based on this literature review. On the other hand, heat sinks are becoming more applicable in industry like cooling of electronic devices, but there is few work done to analyzed their heat transfer behavior. In present study, the magnetohydrodynamic mixed convection of the Al₂O₃-Cu/Water Hybrid Nanofluid is studied considering the heat sink/source. To the knowledge of the authors, this is the first time that the MHD mixed convection of hybrid nanofluid is done for the L shape enclosure by considering the sink/source heat and the effect of its length on heat transfer performance.

2. Mathematical modeling and numerical scheme

Here the mixed convection flow field inside a cavity with side length H filled with Al_2O_3 /water nanofluid and Al_2O_3 -Cu/water hybrid nanofluid, as portrayed in Fig. 1. The flow is considered to be steady, laminar, incompressible, and two dimensions

sional. Moreover, the effects of radiation are neglected to simplify the calculations. The flow is Newtonian and there is no viscous dissipation. Besides, the variations in fluid properties are also neglected for simplification except for density change which is modeled by Boussinesq approximation. Flow Thermo-physical options are expressed in Table 1. Under these assumptions and Boussinesq approximation, one can write the governing equations as [48]:

$$\frac{\partial v}{\partial v} + \frac{\partial u}{\partial x} = 0 \tag{1}$$

$$v\frac{\partial u}{\partial y} + u\frac{\partial u}{\partial x} = -\frac{1}{\rho_{nf}}\frac{\partial p}{\partial x} + \frac{\sigma_n B_0^2}{\rho_{nf}}(v\sin\Phi\cos\Phi - u\sin^2\Phi) + v_{nf}(\frac{\partial^2 u}{\partial x^2} + \frac{\partial^2 u}{\partial y^2})$$
(2)

$$\begin{split} u\frac{\partial v}{\partial x} + v\frac{\partial v}{\partial y} &= -\frac{1}{\rho_{nf}}\frac{\partial p}{\partial y} + v_{nf}(\frac{\partial^2 v}{\partial x^2} + \frac{\partial^2 v}{\partial y^2}) + \frac{\sigma_{nf}B_0^2}{\rho_{nf}}(u\sin\Phi\cos\Phi - v\cos^2\Phi) \\ &\quad + \frac{(\rho\beta)_{nf}}{\rho_{nf}}g(T - T_c) \end{split}$$

(3)

$$v\frac{\partial T}{\partial y} + u\frac{\partial T}{\partial x} = \frac{Q_0}{(\rho c_p)_{uf}} (T - T_c) + \alpha_{nf} (\frac{\partial^2 T}{\partial x^2} + \frac{\partial^2 T}{\partial y^2})$$
(4)

And the boundary conditions are as:

$$x=0, u=v=0, \frac{\partial T}{\partial x}=-\frac{q''}{k_{nf}} \ , \ 0\leqslant y\leqslant l_2 \, , \ and \ \frac{\partial T}{\partial x}$$

=0, otherwise

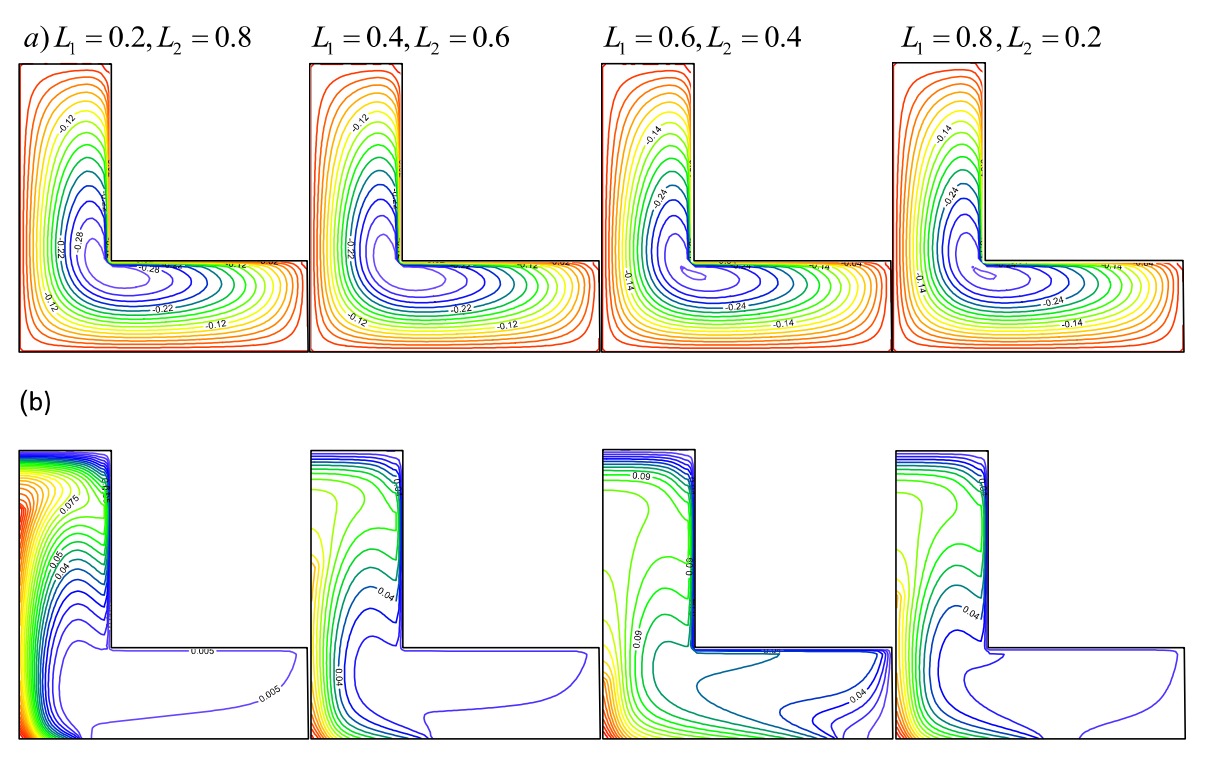


Fig. 3 Contours of streamlines (a), and isotherms (b) for Al_2O_3 —Cu/water Hybrid Nanofluid a $\phi = 0.05, Ha = 10, Q = 1, L = 0.3, \Phi = 45^{\circ}, \lambda_t = -\lambda_r = -1.$

(5)

$$x = l$$
, $u = 0$, $v = \lambda_r U_0$, $\frac{\partial T}{\partial x} = 0$

x = H, u = v = 0, $T = T_C$ at $0 \le y \le l$

$$y = 0$$
, $u = v = 0$, $\frac{\partial T}{\partial y} = -\frac{q''}{k_{nf}}$, $0 \leqslant x \leqslant l_1$, and $\frac{\partial T}{\partial y}$
= 0, otherwise

0.77

$$y = l, \ u = \lambda_t U_0, \quad v = 0 \ , \ \frac{\partial T}{\partial y} = 0$$

$$y = H, \quad T = T_C. \quad u = v = 0$$

2.1. Thermophysical features of regular and hybrid nanofluid

The effectual features of the H_2O/Al_2O_3 nanoliquid and $H_2O/Al_2O_3\text{-}Cu$ hybrid nanoliquid are expressed as follows:

$$\rho_{nf} = (1 - \phi)\rho_{bf} + \phi\rho_{p} \tag{6}$$

$$\rho_{hnf} = \phi_{Cu}\rho_{Cu} + \phi_{Al_2O_3}\rho_{Al_2O_3} + (1 - \phi)\rho_{bf} \tag{7}$$

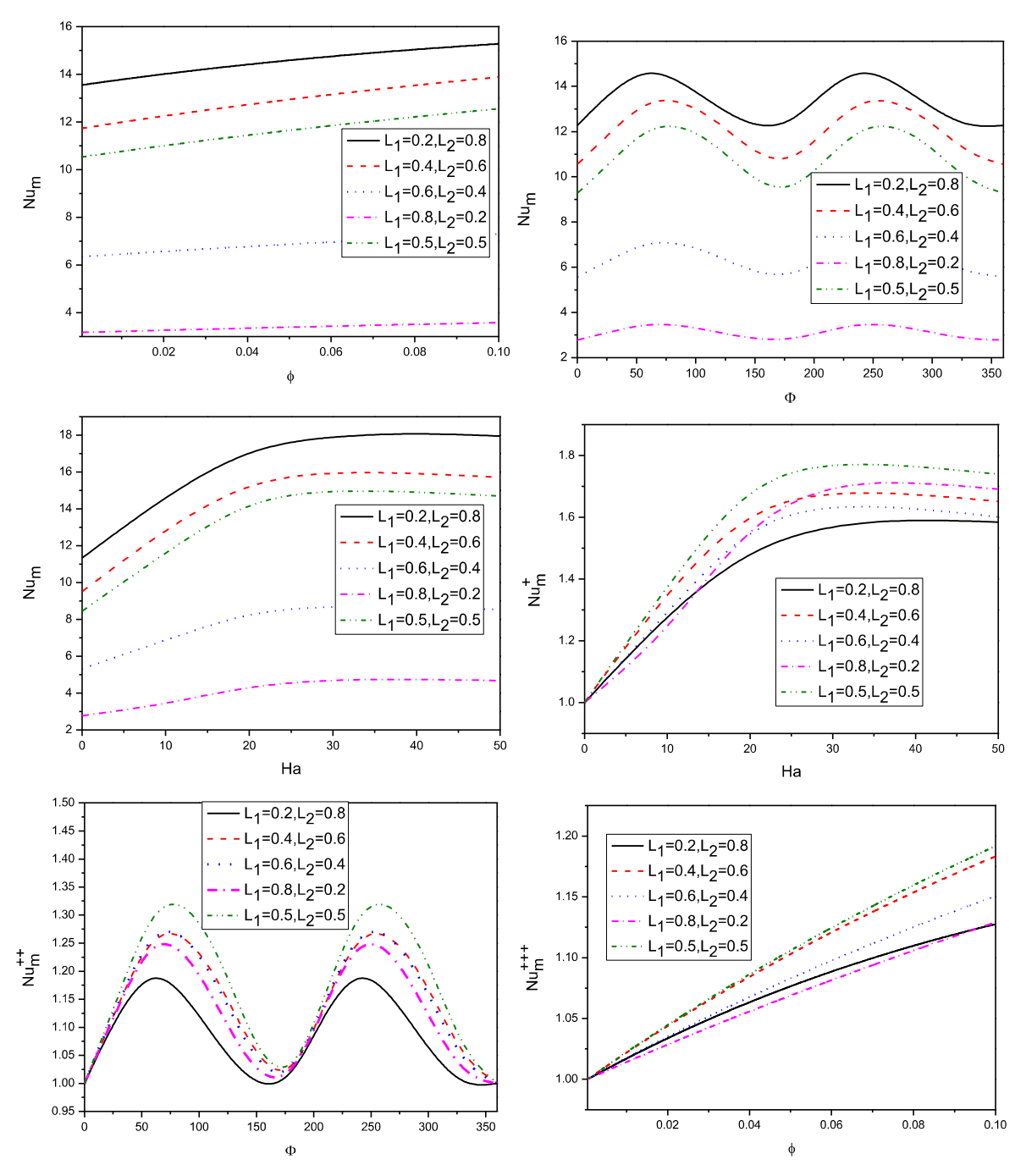


Fig. 5 Variation of the average Nusselt number for Al₂O₃-Cu/water Hybrid Nanofluid at $\phi=0.05,\ Ha=10,\ Q=1, L=0.3, \Phi=45^{\rm O}, \lambda_t=-\lambda_r=-1.$

In Eq. (7) ϕ denotes the whole volume concentration of two diverse kinds of nanoparticles which are dispersed in hybrid nanoliquid and is determined as; $\phi = \phi_{Cu} + \phi_{Al_2O_3}$,

The heat capacitance are given as,

$$(\rho C_p)_{nf} = \phi(\rho C_p)_p + (1 - \phi)(\rho C_p)_{bf}$$
 (8)

$$(\rho C_p)_{hnf} = \phi_{Cu}(\rho C_p)_{Cu} + \phi_{Al_2O_3}(\rho C_p)_{Al_2O_3} + (1 - \phi)(\rho C_p)_{bf}$$

The next coefficient is thermal expansion and is defined:

$$(\rho\beta)_{nf} = (1 - \phi)(\rho\beta)_{bf} + \phi(\rho\beta)_{p} \tag{9}$$

$$(\rho\beta)_{hnf} = \phi_{Al_2O_3}(\rho\beta)_{Al_2O_3} + \phi_{Cu}(\rho\beta)_{Cu} + (1 - \phi)(\rho\beta)_{bf}$$
 (10)

Thermal diffusivity is defined as:

$$\alpha_{nf} = \frac{k_{nf}}{(\rho c_p)_{nf}} \tag{11}$$

$$\alpha_{hnf} = \frac{k_{hnf}}{(\rho C_p)_{hnf}} \tag{12}$$

Thermal conductivity of hybrid nanofluid is proposed:

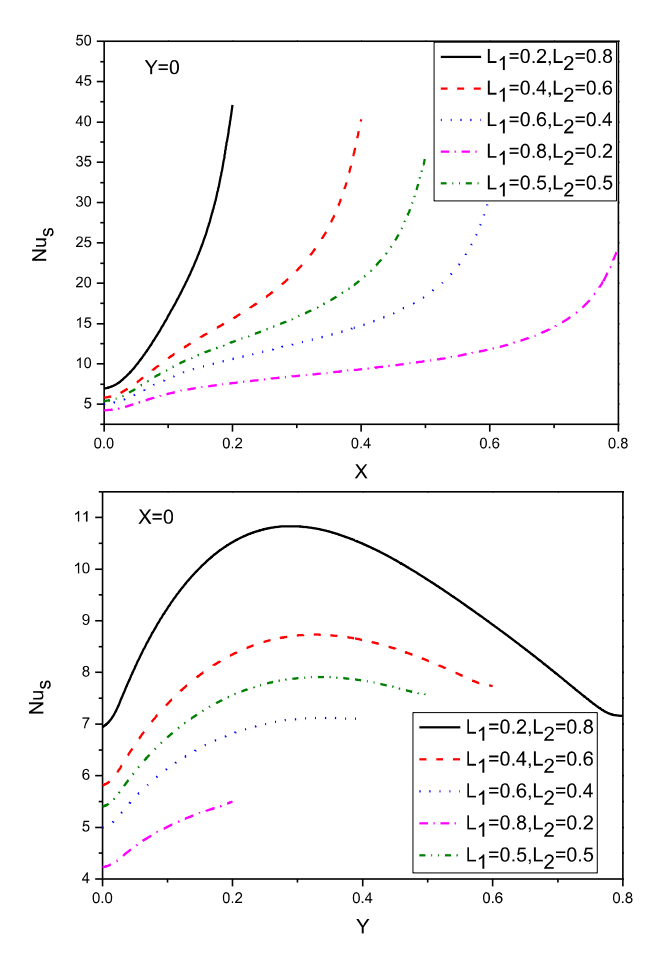
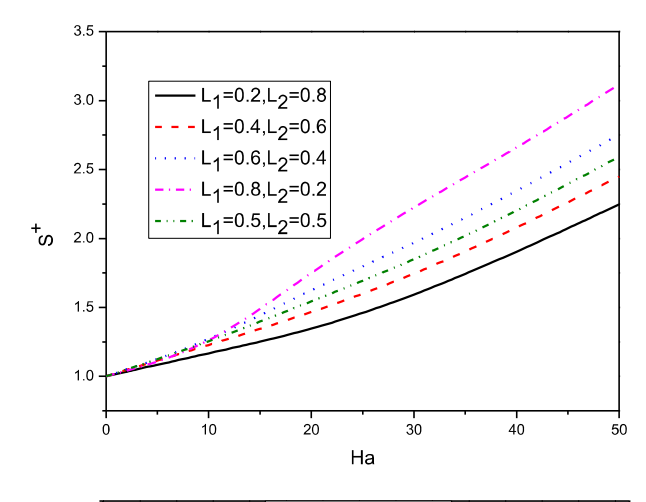
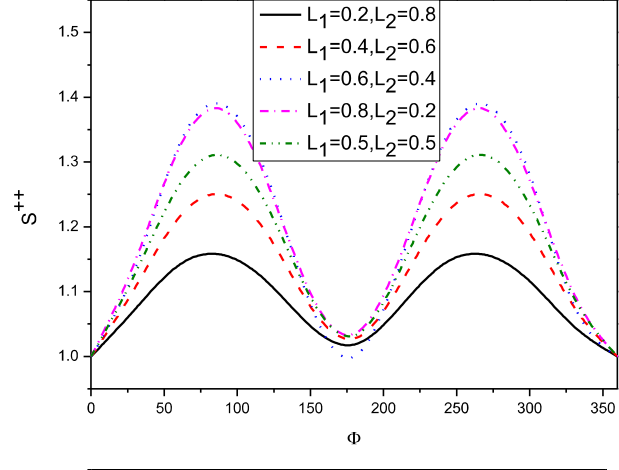


Fig. 4 Profiles of the local Nusselt number along the heat source for Al₂O₃-Cu/water Hybrid Nanofluid at $\phi = 0.05$, Ha = 10, Q = 1, L = 0.3, $\Phi = 45^{\circ}$, $\lambda_t = -\lambda_r = -1$.





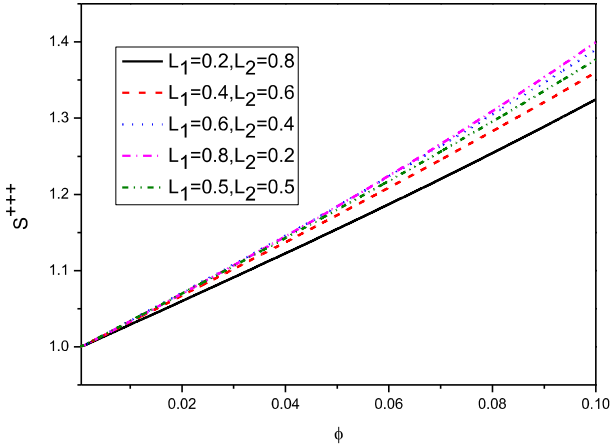


Fig. 6 Variation of the average total entropy generation for Al_2O_3 —Cu/water Hybrid Nanofluid at $\Phi=45^O,$ $\phi=0.05, Q=1, L=0.3, \lambda_t=-\lambda_r=-1.$

$$\frac{k_{hnf}}{k_{hf}} = \left(\frac{\left(\phi_{Cu} k_{Cu} + \phi_{Al_2O_3} k_{Al_2O_3} \right)}{\phi} + 2k_{hf} + 2\left(\phi_{Al_2O_3} k_{Al_2O_3} + \phi_{Cu} k_{Cu} \right) - 2\phi k_{hf} \right) \\
\times \left(\frac{\left(\phi_{Al_2O_3} k_{Al_2O_3} + \phi_{Cu} k_{Cu} \right)}{\phi} - \left(\phi_{Cu} k_{Cu} + \phi_{Al_2O_3} k_{Al_2O_3} \right) + 2k_{hf} + \phi k_{hf} \right)^{-1} \tag{13}$$

The form of effective dynamic viscosity of the regular nanofluid and also hybrid nanofluid is given by:

$$\mu_{nf} = \frac{\mu_{bf}}{(1 - \phi)^{2.5}} \tag{14}$$

$$\mu_{hnf} = \frac{\mu_{bf}}{\left(1 - \left(\phi_{Al_2O_3} + \phi_{Cl_2}\right)\right)^{2.5}} \tag{15}$$

And the effective electrical conductivity is expressed as:

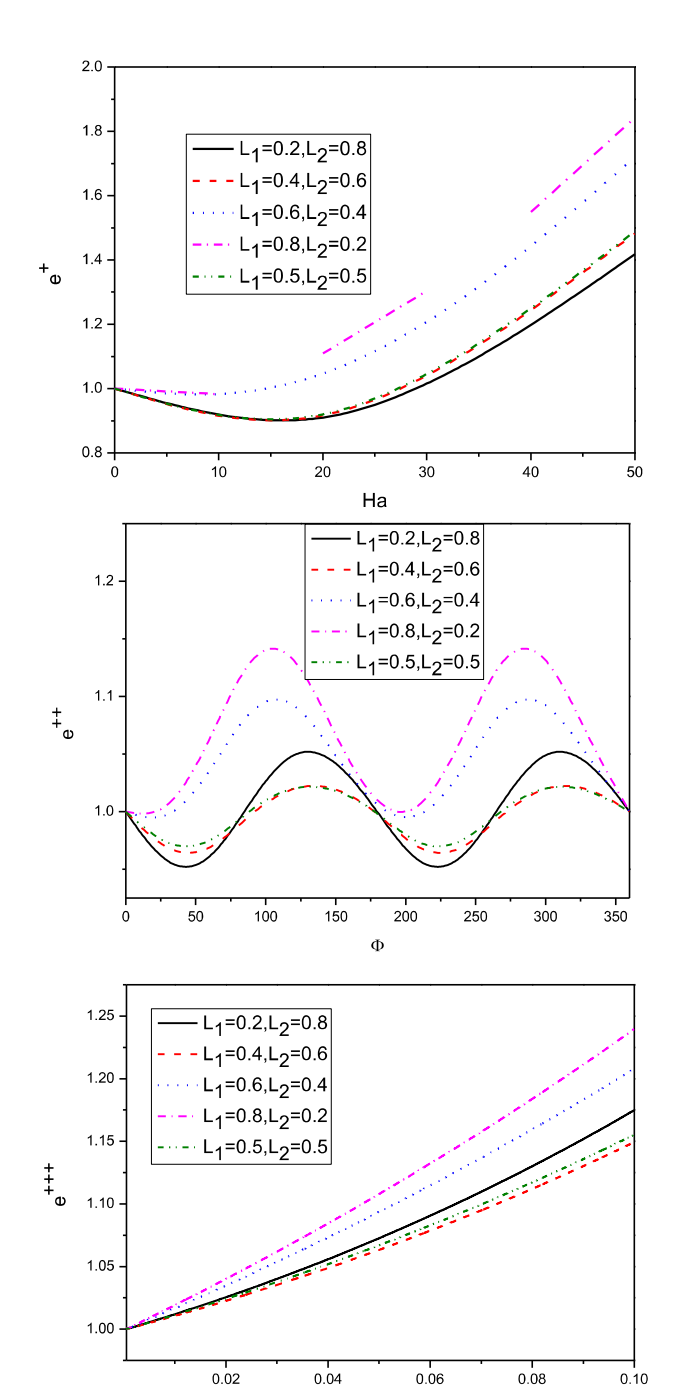


Fig. 7 Variation of global entropy to average Nusselt number for Al₂O₃-Cu/water Hybrid Nanofluid at $\phi = 0.05, Ha = 10$, $\Phi = 45^{\circ}, Q = 1, L = 0.3, \lambda_t = -\lambda_r = -1$.

$$\frac{\sigma_{nf}}{\sigma_{bf}} = 1 + \frac{3\left(\frac{\sigma_p}{\sigma_{bf}} - 1\right)\phi}{\left(\frac{\sigma_p}{\sigma_{bf}} + 2\right) - \left(\frac{\sigma_p}{\sigma_{bf}} - 1\right)\phi} \tag{16}$$

$$\frac{\sigma_{hnf}}{\sigma_{bf}} = 1 + \frac{3\left(\frac{\left(\phi_{Cu}\sigma_{Cu} + \phi_{Al_2O_3}\sigma_{Al_2O_3}\right)}{\sigma_{bf}} - \left(\phi_{Cu} + \phi_{Al_2O_3}\right)\right)}{\left(\frac{\left(\phi_{Cu}\sigma_{Cu} + \phi_{Al_2O_3}\sigma_{Al_2O_3}\right)}{\phi\sigma_{bf}} + 2\right) - \left(\frac{\left(\phi_{Cu}\sigma_{Cu} + \phi_{Al_2O_3}\sigma_{Al_2O_3}\right)}{\sigma_{bf}} - \left(\phi_{Cu} + \phi_{Al_2O_3}\right)\right)}{\left(17\right)}$$

Considering the following parameters:

$$X = \frac{x}{H}, \quad Y = \frac{y}{H}, \quad V = \frac{y}{U_0}, \quad U = \frac{u}{U_0}, \quad \theta = \frac{(T - T_c)}{\Delta T},$$

$$\Delta T = \frac{q'' \cdot H}{k_f}, \quad P = \frac{p}{\rho_{m'} U_0^2}, \quad Ri = \frac{Gr}{Re^2}$$

$$L = \frac{l}{H}, \quad L_1 = \frac{l}{H}, \quad L_2 = \frac{l_2}{H}$$
(18)

The governing equations change to the following ones:

$$\frac{\partial V}{\partial Y} + \frac{\partial U}{\partial X} = 0 \tag{19}$$

$$U\frac{\partial U}{\partial X} + V\frac{\partial U}{\partial Y} = (\frac{Ha^2}{Re})(\frac{\sigma_{nf}\rho_f}{\sigma_f\rho_{nf}})(V\sin\Phi\cos\Phi - U\sin^2\Phi)$$
$$-\frac{\partial P}{\partial X} + \frac{1}{Re}(\frac{v_{nf}}{v_e})(\frac{\partial^2 U}{\partial Y^2} + \frac{\partial^2 U}{\partial X^2}) \tag{20}$$

$$\begin{split} V\frac{\partial V}{\partial Y} + U\frac{\partial V}{\partial X} &= -\frac{\partial P}{\partial Y} + \frac{1}{Re} \binom{v_{nf}}{v_{f}} \left(\frac{\partial^{2} V}{\partial Y^{2}} + \frac{\partial^{2} V}{\partial X^{2}} \right) \\ &+ \binom{\sigma_{nf}}{\sigma_{f}} \binom{\rho_{f}}{\rho_{nf}} \frac{Ha^{2}}{Re} \left(U \sin\Phi \cos\Phi - V \cos^{2}\Phi \right) + Ri \frac{(\rho\beta)_{nf}}{\rho_{nf} \beta_{f}} \theta \end{split} \tag{21}$$

$$V\frac{\partial\theta}{\partial Y} + U\frac{\partial\theta}{\partial X} = (\frac{\alpha_{nf}}{\alpha_f})(\frac{1}{\Pr.Re})(\frac{\partial^2\theta}{\partial Y^2} + \frac{\partial^2\theta}{\partial X^2}) + \frac{(\rho c_p)_f}{(\rho c_p)_{nf}} \frac{1}{Re.\Pr}Q\theta$$
(22)

Where $Ha=B_0H\sqrt{\sigma_f/\mu_f}$, $Re=\frac{U_0\,H}{v_f}$, $Gr=\frac{g\beta_f\,H^3\Delta T}{v_f^2}$, $Pr=\frac{v_f}{z_f}$ are respectively the Hartmann, Grashof, Reynolds, and Prandtl numbers

And the non-dimensional boundary conditions:

$$X = 0, U = V = 0, \frac{\partial \theta}{\partial X} = -\frac{k_f}{k_{nf}}, 0 \leqslant Y \leqslant L_2 \text{ and } \frac{\partial \theta}{\partial X}$$

= 0, otherwise

$$X = L, \ U = 0, \ V = \lambda_r, \ \frac{\partial \theta}{\partial X} = 0$$

$$X = 1$$
, $U = V = 0$, $\theta = 0$ at $0 \leqslant Y \leqslant L$

$$Y = 0, U = V = 0, \frac{\partial \theta}{\partial Y} = -\frac{k_f}{k_{nf}}, \ 0 \leqslant X \leqslant L_1, \ and \ \frac{\partial \theta}{\partial Y}$$

= 0, otherwise (23)

$$Y = L, \ U = \lambda_t, \ V = 0, \ \frac{\partial \theta}{\partial Y} = 0$$

$$Y = 1, \ \theta = 0 \ U = V = 0.$$

The local Nusselt number is expressed as:

$$(Nu_s)_{Y=0} = \frac{1}{\theta_s(X)}, \quad (Nu_s)_{X=0} = \frac{1}{\theta_s(Y)}$$
 (24)

And for average Nusselt number one has:

$$Nu_m = \frac{Nu_{ml} + Nu_{md}}{2}$$

Where

$$Nu_{ml} = \frac{1}{L_2} \int_0^{L_2} Nu_l \, dY, \ Nu_{md} = \frac{1}{L_1} \int_0^{L_1} Nu_r \, dX$$
 (25)

2.2. Entropy generation analysis

The dimensionless form of total local entropy generation can be stated by:

$$S = s \cdot \frac{H_{2}}{k_{f}} = \left(\frac{k_{nf}}{k_{f}}\right) \cdot \frac{1}{(\theta + C_{T})^{2}} \left[\left(\frac{\partial \theta}{\partial Y}\right)^{2} + \left(\frac{\partial \theta}{\partial X}\right)^{2}\right] +$$

$$\Pr^{2} \cdot Re^{2} \cdot \Theta \cdot \left(\frac{\mu_{nf}}{\mu_{f}}\right) \cdot \left\{2\left[\left(\frac{\partial V}{\partial Y}\right)^{2} + \left(\frac{\partial U}{\partial X}\right)^{2}\right] + \left(\frac{\partial U}{\partial Y} + \frac{\partial V}{\partial X}\right)^{2}\right\}$$

$$+\Theta \cdot Re^{2} \cdot \Pr^{2} \cdot \left(\frac{\sigma_{nf}}{\sigma_{f}}\right) \cdot \left(-V\cos\Phi + U\sin\Phi\right)^{2} \cdot Ha^{2}$$

$$= Sh + Sv + Sj$$

$$(26)$$

Where $\Theta = \left(\frac{\alpha_f}{H}\right)^2 \left(\frac{\mu_f}{\Delta T. k_f}\right)$

Here Sh, Sv, and Sj are the non-dimensional local entropy generation rate owing to heat transfer, fluid friction, and Joule heating, respectively.

Also, the following total entropy generation ratio, Nusselt ratio and thermal performance criterion are defined as;

$$Nu_{m}^{+} = \frac{Nu_{m}}{(Nu_{m})_{Ha=0}}, \ Nu_{m}^{++} = \frac{Nu_{m}}{(Nu_{m})_{\Phi=0}}, and \ Nu_{m}^{+++}$$

$$= \frac{Nu_{m}}{(Nu_{m})\phi \approx 0}$$
(27)

$$S^{+} = \frac{S}{(S)_{Ha=0}}$$
, $S^{++} = \frac{S}{(S)_{\Phi=0}}$, and $S^{+++} = \frac{S}{(S)_{\phi\approx 0}}$ (28)

$$e^{+} = \frac{S^{+}}{Nu_{m}^{+}}, \ e^{++} = \frac{S^{++}}{Nu_{m}^{++}}, \ and \ e^{+++} = \frac{S^{+++}}{Nu_{m}^{+++}}$$
 (29)

These set of equations are solved using FDM and showed very agreement validity with other papers [22,49].

3. Numerical solution and validation

The conservation Eqs. (19)–(22) in conjunction with the associated boundary conditions (23) indicate a system of nonlinear partial differential equations that are robustly coupled. These equations were converted into algebraic equations through the Finite Volume Approach and hence solved iteratively by

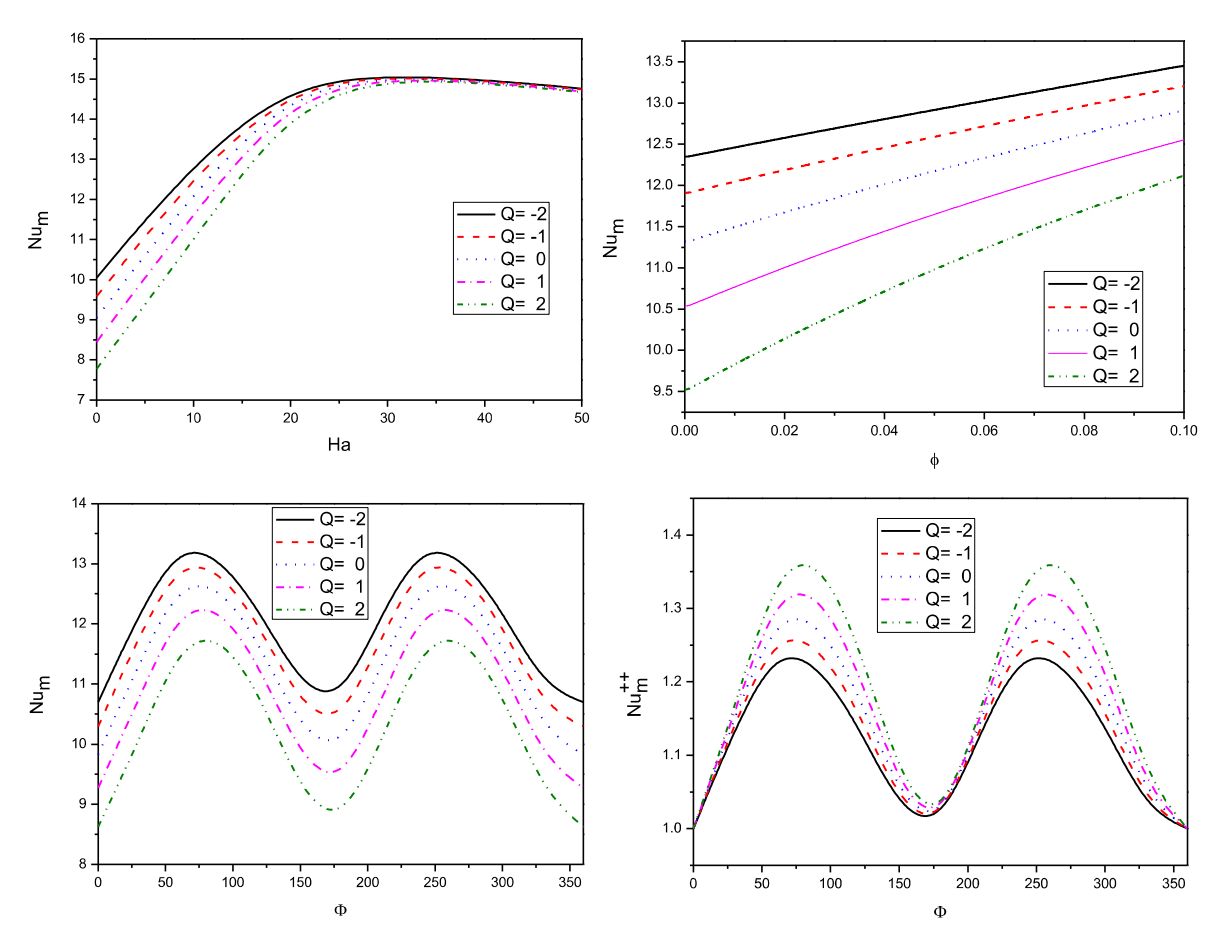


Fig. 8 Variation of the average Nusselt number for Al_2O_3 —Cu/water Hybrid Nanofluid at $\phi = 0.05$, $\Phi = 45^{O}$, $L_1 = L_2 = 0.5$, Ha = 10, L = 0.3, $\lambda_t = -\lambda_r = -1$.

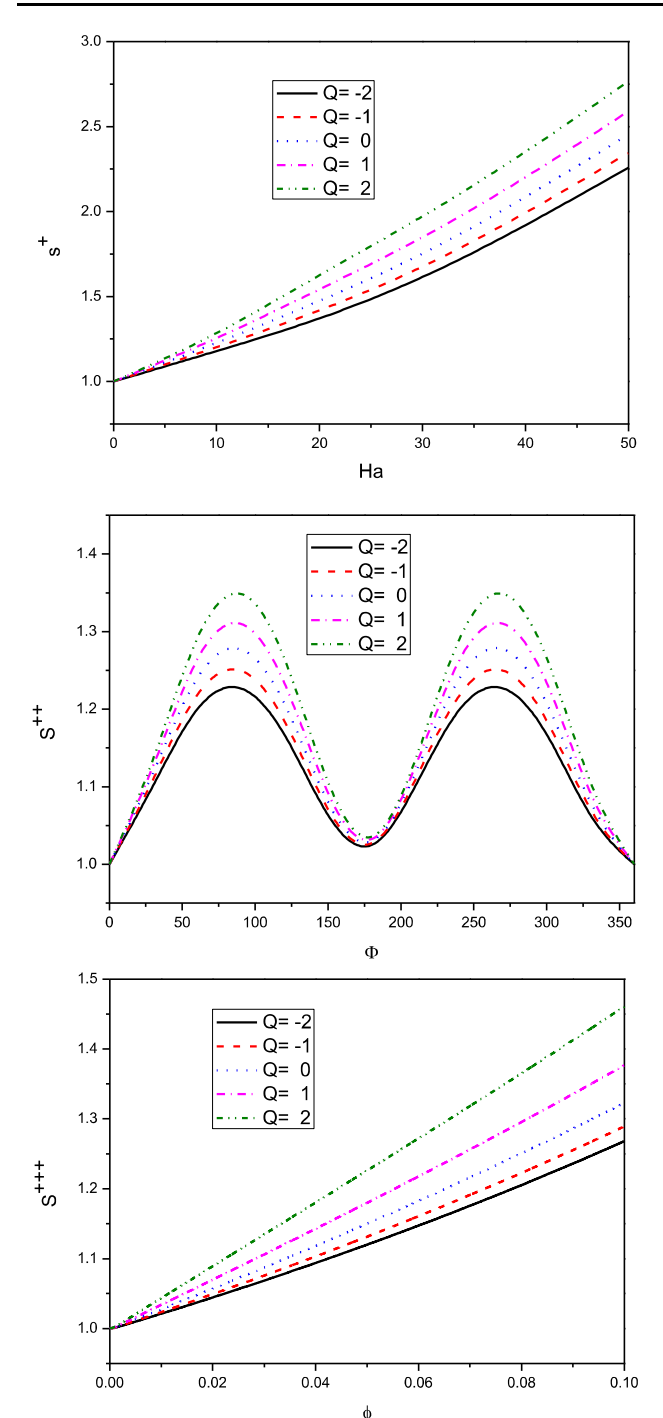


Fig. 9 Variation of the average total entropy generation for Al₂O₃–Cu/water Hybrid Nanofluid at $\phi = 0.05$, $\Phi = 45^{\circ}$, $L_1 = L_2 = 0.5$, Ha = 10, L = 0.3, $\lambda_t = -\lambda_r = -1$.

the tri-diagonal matrix algorithm, utilizing the SIMPLE algorithm [27]. Fig. 2, exhibits the outcomes of the current code which are compared with those of this contribution with those of Khanafar and Chamkha [50] and Iwatsu et al. [51]. The outcomes elucidate an assent between this investigation and the previously cited investigations. For convergence, the underrelaxation technique has been performed. The iteration is reported until the normalized residuals of the mass, momen-

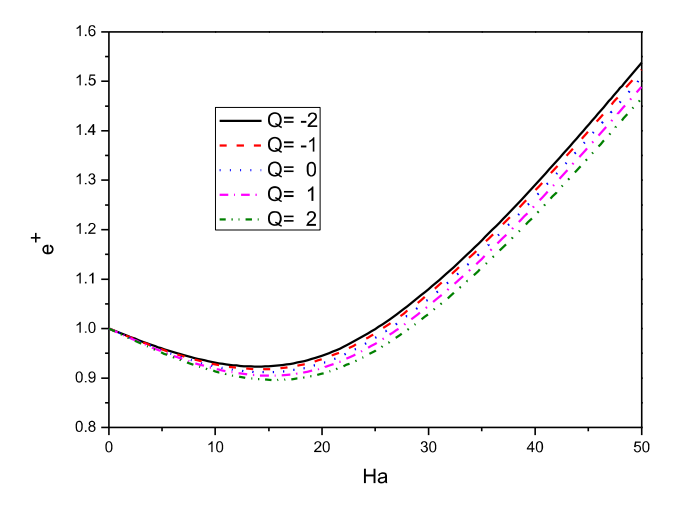


Fig. 10 Variation of global entropy to average Nusselt number for Al₂O₃-Cu/water Hybrid Nanofluid at $\Phi=45^{\rm O},\ \phi=0.05,\ L_1=L_2=0.5, Ha=10, L=0.3, \lambda_t=-\lambda_r=-1.$

tum, temperature and entropy generation equations become less than 10^{-6} . The non-uniform grid contains of 101x101 grid nodes in the *X*-and *Y*-directions, respectively. The obtained results are separated of the number of the grids. The grid independency data are found at

$$\begin{aligned} Ha &= 10, \Theta = 10^{-3}, C_T = 0.1, Gr = 10^4, Re = 10, D = 0.5, B \\ &= 0.5, Q = 1.0, \Phi = 45, \phi = 0.05, \lambda_l = -\lambda_r = 1.0 \end{aligned}$$

and displayed in Table 2.

Also, to show the validity and demonstrate the accuracy of the proposed procedure the numerical computations at specific status are compared with the former outputs obtained by Khanafer and Chamkha [50] and Iwatsu et al. [51] as shown in Table 3. It is manifested that there is a well consensus between the outcomes.

4. Results and discussion

Numerical simulation for mixed convection of the Al₂O₃-Cu/ Water Hybrid Nanofluid heat transfer is done in this paper by considering the MHD effect and the source/sink heat generation. The contours of isotherms and streamlines are considered, in order to observe the patterns of flow and structure of heat transfer regimes. Fig. 3 demonstrates the changes of streamlines and isotherms for different lengths of heater. For studying the sole effect of heater size on isotherms and streamlines, other parameters like volume fraction, Hartmann number, Reynolds number, and the contours are set constant. As seen, changing the heater length has no vivid impact on the streamline since the geometry is symmetric regarding the cold walls and the lengths of heaters. The flow through heaters tends to go upward due to lower density, and come downward from the cold walls. On the other hand, the insulated walls block the coming air and altogether the flow circulates in the cavity and makes vortices. Corresponding temperature distribution patterns are also demonstrated as isotherms. As it is demonstrated, the maximum amount of isotherms is at the corner of the cavity where the heaters exist. The amount of

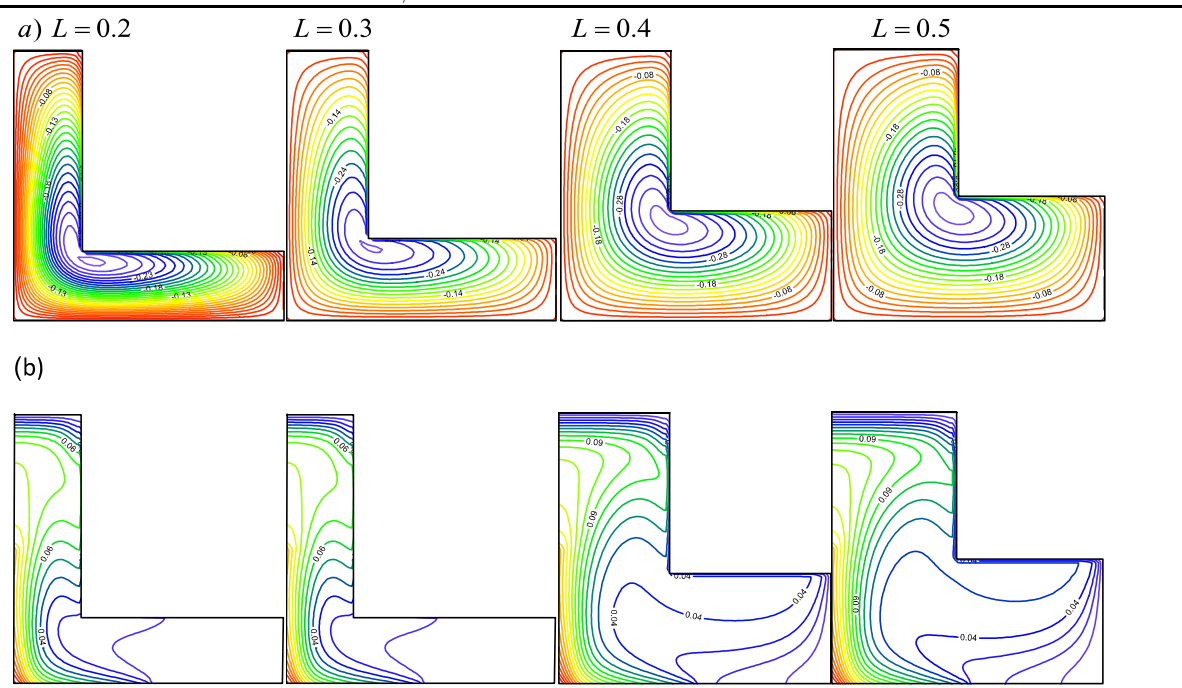
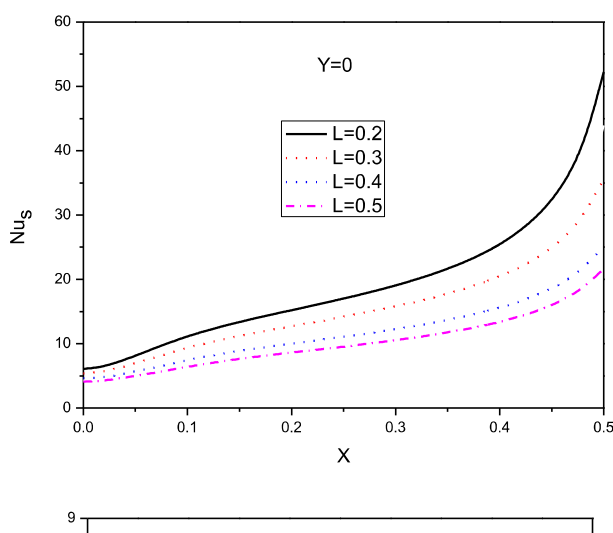


Fig. 11 Contours of streamlines (a), and isotherms (b) for Al₂O₃–Cu/water $\Phi = 45^{\circ}$, $\phi = 0.05$, $L_1 = L_2 = 0.5$, Ha = 10, Q = 1, $\lambda_t = -\lambda_r = -1$.

isotherm change based on the length of heaters. For example, for $L_2=0.8$, the isotherm at the right insulated wall is higher.

In Fig. 4, one can see the changes of Nusselt number for different lengths of heaters for five different modes of the heater length in X and Y directions. The other parameters remain constant so that the sole effect of heater length on Nusselt number can be exhibited. The local Nusselt number increases by increasing the amount of X for each mode. The reason is that the negative effect of vertical heater is reduced by becoming far from the vertical wall. On the other hand, increasing the length of L₁ reduced the local Nusselt number at the fixed position of X. this is due to reducing the blocking effect of horizontal heater on heat transfer. If one walks on the vertical wall, the Nusselt number increases and then decreases for all of the modes.

The changes of average Nusselt number versus nanoparticle volume fraction (Fig. 5-a), Hartmann number (Fig. 5-b), inclination angle (Fig. 4-c) and also the Nusselt ratios (Nu + m, Nu + + m, Nu + + + m) are depicted in Fig. 5 for various lengths of heaters on side bottom walls. By increasing the solid volume fraction, the thermal conductivity of nanofluid improves and so the average Nusselt number increases. The non-dimensional average Nusselt number on the heaters is the increasing function of the Hartmann number, and the magnetic field angle has the sinusoidal impact on Nusselt number. The reason for this sinusoidal behavior is the form of magnetic field angle in Navier-Stockes equations (Eqs. (2) and (3)). The magnetic field reduces the buoyancy force and so is the controlling parameter. As mentioned, total entropy generation is sum of three types; heat transfer, joule heating, and fluid fraction and is shown in Fig. 6 and Fig. 7. Entropy increases by the Hartmann number, which means that the entropy generation due to magnetic force is increased, and solid volume fraction and also again is sinusoidal for the changes of magnetic field angle.



Hybrid

Nanofluid

at

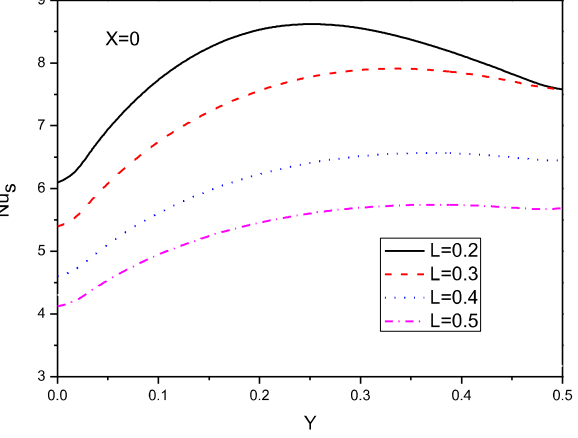


Fig. 12 Profiles of the local Nusselt number along the heat source for Al₂O₃–Cu/water Hybrid Nanofluid at $\phi = 0.05$, Ha = 10, $L_1 = L_2 = 0.5$, $\Phi = 45^{\rm O}$, Q = 1, $\lambda_t = -\lambda_r = -1$.

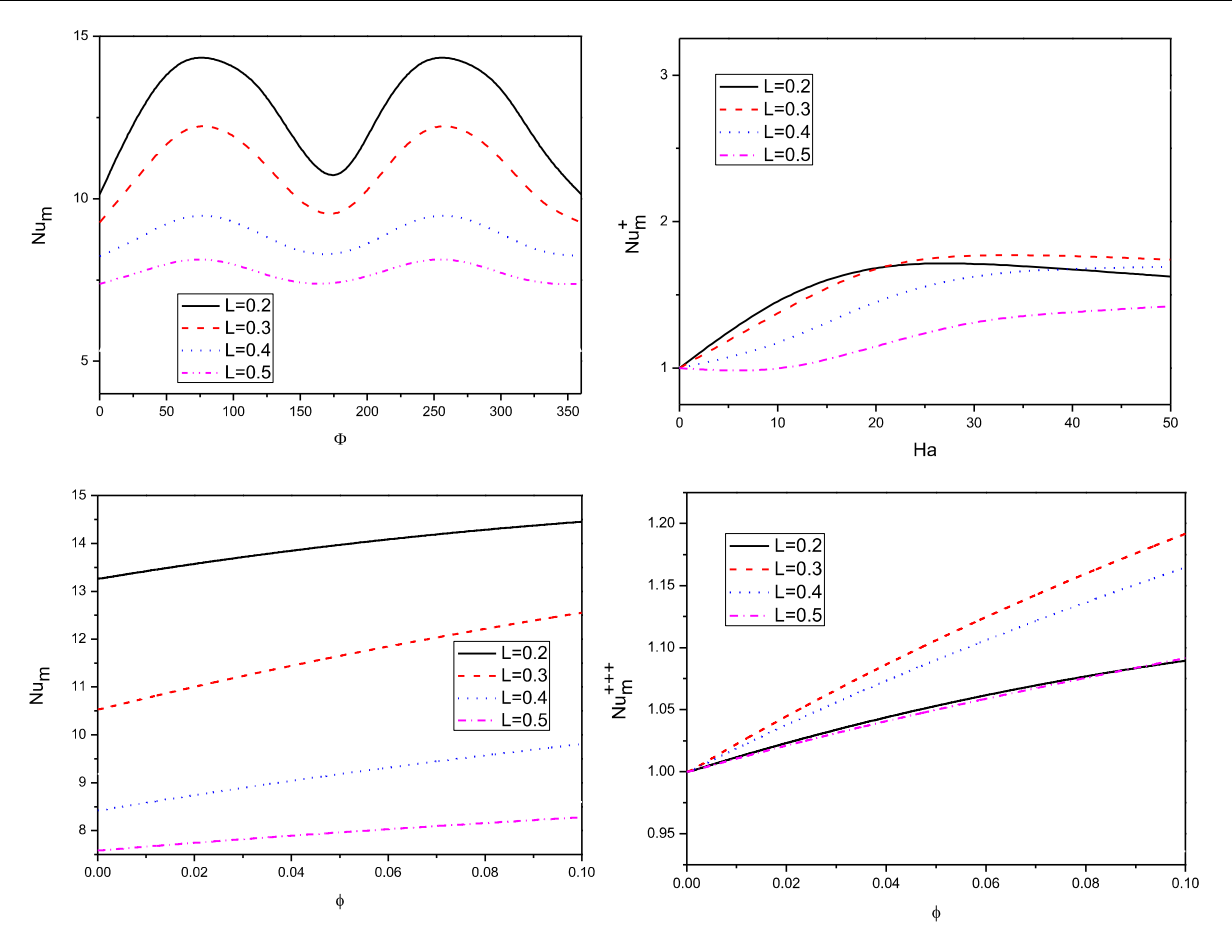


Fig. 13 Variation of the average Nusselt number for Al₂O₃–Cu/water Hybrid Nanofluid at $\phi = 0.05$, $\Phi = 45^{\circ}$, $L_1 = L_2 = 0.5$, Ha = 10, $\lambda_t = -\lambda_r = -1$, Q = 1.

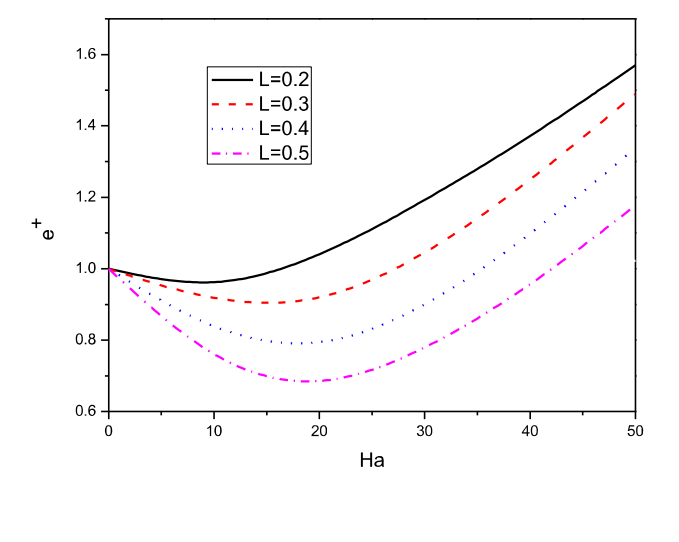
Figs. 8–10 are shown the impacts of internal heat sink/source on normalized heat transfer, entropy generation and thermal performance. Remarkable points related to the variations of Nu number with different parameters of Fig. 8 are as follow:

With the increase of Ha up to around Ha = 20, Nu number increases for all amounts of Q. After Ha = 20, Q will indicate a decreasing rate. For all amounts of Q, the maximum values of Nu will be observed at the ranges of $\Phi \cong (65-75)$ and also $\Phi \cong (240-260)$ degrees. Apart from $\Phi \cong 0$ and $\Phi \cong 360$, there is a relative minimum point for the range of $\Phi \cong (170-175)$. In other words, the angles of 60 and 240 are the most effective ones in order to impose magnetic field, while the angle of 180 is the optimum one provided the decrease of heat transfer is desirable.

Nu number increases with the increment of volume fraction and for Q=2, the rate of increase is more than that for all other amounts of Q. Similarly, in comparison with other amounts of Q, Q=2 is mostly influenced by variations of the angle of imposing magnetic field. The increment of heat transfer causes increasing of irreversibility regarding heat transfer, and considering that in such matters, the main portion of entropy generation is related to irreversibility due to heat transfer, it is therefore expected from Fig. 8 that, for the whole values of Q, entropy generation increases with the

increase of Φ . On the other hand, the increase of Ha brings Jule heating irreversibility, and so entropy generation increments with the increase of Ha. As shown in Fig. 10 very remarkable point is; At Ha < 20, imposing the magnetic field can be improved the thermal performance criteria for all values of Q. Fig. 11 shows isotherm and streamlines for different numbers of aspect ratio. As a result of the location of hot wall, streamlines have a CW rotation and will become maximum at the right corner within the cavity. At isothermal lines, dimensionless temperature goes up with the increment of aspect ratio and considering its definition, Nu number decreases, so that local Nu number is shown in Fig. 12. The maximum value of local Nu is related to horizontal hot wall and occurs at the end of it, and considering the aforementioned explanations, the maximum amount of local Nu belongs to L = 0.2. Fig. 13 shows the variations of mean Nu number and normalized Nu for different variables and different amounts of aspect ratio. Remarkable points in these figures are as follow:

With the decrease of aspect ratio (L), the effects of angle changing on heat transfer increases remarkably. The increment of volume fraction leads to increasing of heat transfer for all amounts of L. At L=0.5, the rate of increase according to the increase of volume fraction is more than that of all other amounts of L. As a highly remarkable point, at L=0.5, heat transfer decreases via increasing the Ha number. This means



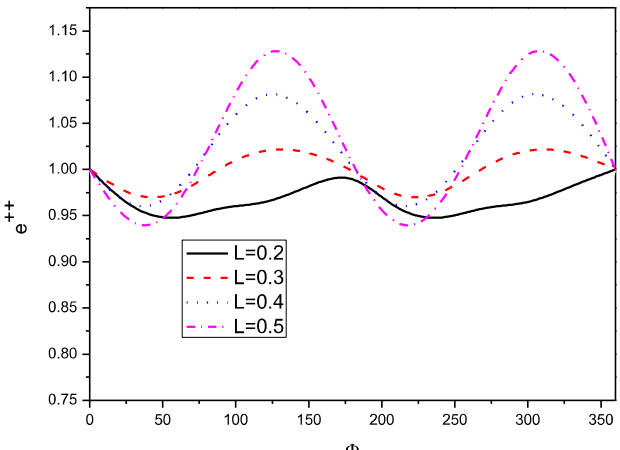


Fig. 14 Variation of global entropy to average Nusselt number for Al₂O₃–Cu/water Hybrid nanofluid at $\phi = 0.05$, $\Phi = 45^{\circ}$, $L_1 = L_2 = 0.5$, Ha = 10, $L_2 = -1$, Ha = 10, $L_3 = -1$, $L_4 = -1$, $L_5 = -1$,

that by approaching to the form of square cavity, the same results mentioned in many articles will be observed; "decreasing Nu via increasing Ha".

But for small amounts of L, there is a heat transfer increase with the increment of Ha. Fig. 14 reveals the variations of normalized thermal performance with different values of Ha and Φ. In general, a better thermal performance is observed at high value of L and low value of Ha, while the optimum state occurs at Ha < 20. About thermal performance of L-Shaped cavity at different amounts of L, some important points could be mentioned; in general, at L = 0.2, imposing magnetic field at all angles causes the enhancement of thermal performance. For other values of L, imposing magnetic field at the angles of 0-60 and 200-250 degree causes the enhancement of thermal performance but for other angles it leads to the decrease of thermal performance. Figs. 15–17 show the effects of different movement direction of the moving walls on thermal performance and heat transfer. For both horizontal and vertical hot walls, the maximum and minimum amounts of local Nu are based on $\lambda_t = -\lambda_r = -1$ and $\lambda_t = -\lambda_r = 1$, respectively. Fig. 16 shows the rate of increase of heat transfer with the

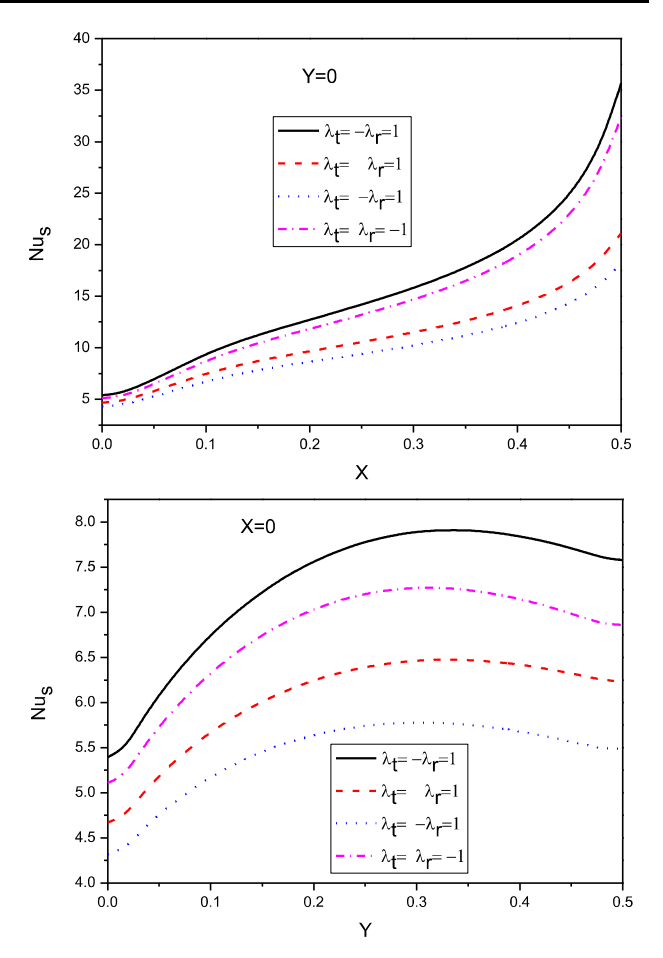


Fig. 15 Profiles of the local Nusselt number along the heat source for Al₂O₃-Cu/water Hybrid Nanofluid at $\phi = 0.05$, $\Phi = 45^{\circ}$, $L_1 = L_2 = 0.5$, Ha = 10, L = 0.3, Q = 1.

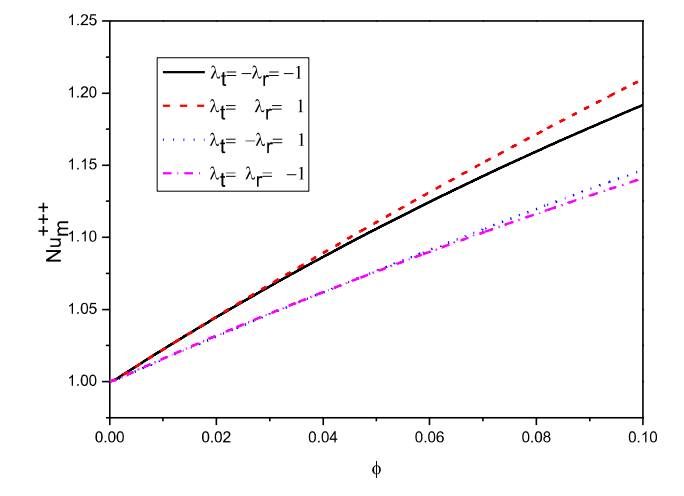


Fig. 16 Variation of the average Nusselt number for Al₂O₃–Cu/water Hybrid Nanofluid at $\phi = 0.05$, $\Phi = 45^{O}$, $L_1 = L_2 = 0.5$, Ha = 10, L = 0.3, Q = 1.

increment of volume fraction in nanoparticles. Addition of nanoparticles has the maximum and minimum influences at the states of $\lambda_t = \lambda_r = 1$ and $\lambda_t = \lambda_r = -1$, respectively. For

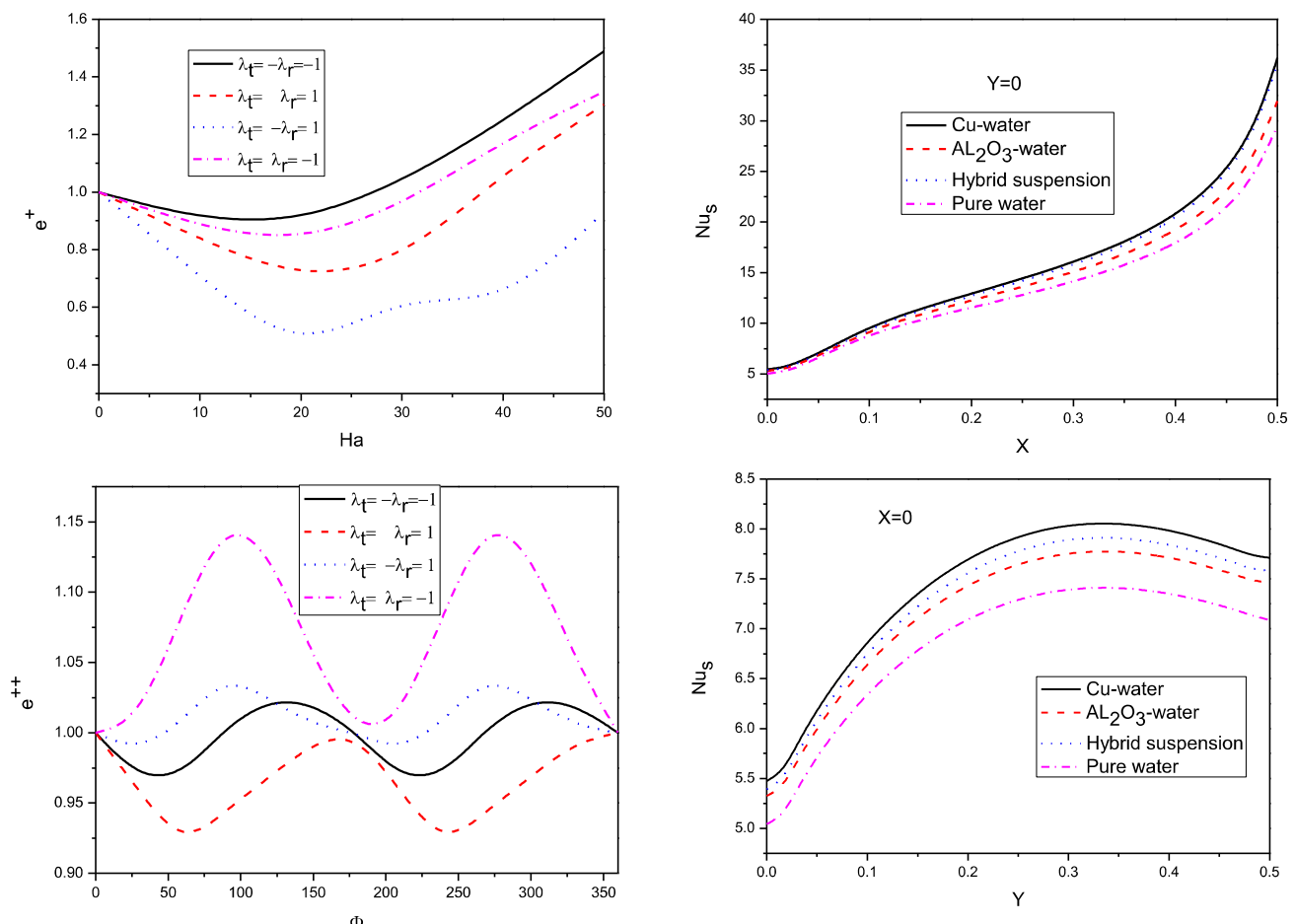


Fig. 17 Variation of global entropy to average Nusselt number for Al₂O₃ –Cu/water Hybrid Nanofluid at $\phi=0.05, \Phi=45^{\rm O}, L_1=L_2=0.5, Ha=10, Q=1, L=0.3$.

 $\lambda_t = -\lambda_r = 1$, imposing magnetic field leads to the improvement of thermal performance, while for other states, addition of magnetic field up to around Ha = 30, causes the enhancement of thermal performance. Imposing magnetic field for $\lambda_t = \lambda_r = -1$ leads to the reduction of thermal performance and this reduction can be observed at all angles of imposing magnetic field. For other states of movement, imposing magnetic field with tiny angles at the first and third quarter causes the enhancement of thermal performance. For $\lambda_t = \lambda_r = 1$ at all angles, improvement of thermal performance for various angles can be observed. It may be claimed that imposing magnetic field has the best function in the improvement of thermal performance of $\lambda_t = \lambda_r = 1$. Fig. 18 offers a comparison of local Nu among Cu-Water, Hybrid nanofluid, pure water, and Al2O3-water. As observed in the figure, the maximum amount of heat transfer is seen at the Cu-Water nanofluid, after which hybrid has the highest amount of heat transfer. Considering Fig. 19, it can be claimed that for all 4 fluids, imposing magnetic field leads to the enhancement of thermal performance, while the best performance is related to hybrid.

Fig. 18 Profiles of the local Nusselt number along the heat source for types of Nanfluid at $\phi = 0.05$, Ha = 10, L = 0.3, $\Phi = 45^{\circ}$, $L_1 = L_2 = 0.5$, $\lambda_t = -\lambda_r = -1$, Q = 1.

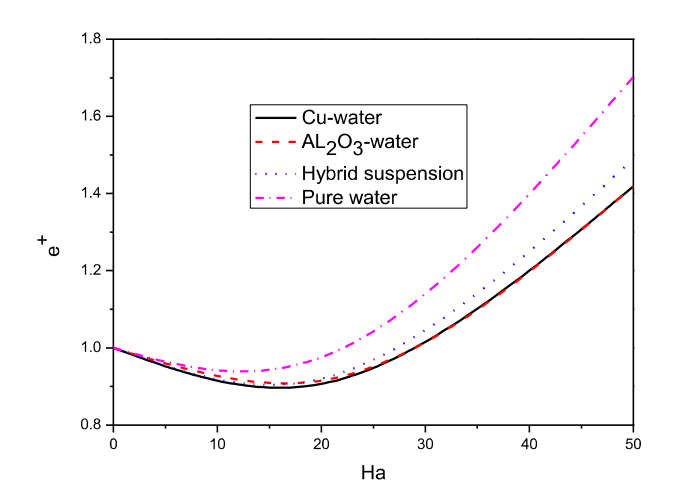


Fig. 19 Variation of global entropy to average Nusselt number for types of Nanofluid at $\phi=0.05, L=0.3, \Phi=45^{\rm O}, L_1=L_2=0.5, \lambda_t=-\lambda_r=-1, Q=1.$